1-2016

Machine-Vision-Based Roadway Health Monitoring and Assessment: Development of a Shape-Based Pavement-Crack-Detection Approach

Kasthurirangan Gopalakrishnan
Iowa State University, USA, rangan@iastate.edu

Omar G. Smadi
Iowa State University, smadi@iastate.edu

Halil Ceylan
Iowa State University, hceylan@iastate.edu

Koray Celik
Iowa State University, koray@iastate.edu

Arun K. Somani
Iowa State University, arun@iastate.edu

Machine-Vision-Based Roadway Health Monitoring and Assessment: Development of a Shape-Based Pavement-Crack-Detection Approach

Final Report
January 2016

Sponsored by
Midwest Transportation Center
U.S. Department of Transportation
Office of the Assistant Secretary for
Research and Technology

IOWA STATE UNIVERSITY
Institute for Transportation

About MTC

The Midwest Transportation Center (MTC) is a regional University Transportation Center (UTC) sponsored by the U.S. Department of Transportation Office of the Assistant Secretary for Research and Technology (USDOT/OST-R). The mission of the UTC program is to advance U.S. technology and expertise in the many disciplines comprising transportation through the mechanisms of education, research, and technology transfer at university-based centers of excellence. Iowa State University, through its Institute for Transportation (InTrans), is the MTC lead institution.

About InTrans

The mission of the Institute for Transportation (InTrans) at Iowa State University is to develop and implement innovative methods, materials, and technologies for improving transportation efficiency, safety, reliability, and sustainability while improving the learning environment of students, faculty, and staff in transportation-related fields.

ISU Non-Discrimination Statement

Iowa State University does not discriminate on the basis of race, color, age, ethnicity, religion, national origin, pregnancy, sexual orientation, gender identity, genetic information, sex, marital status, disability, or status as a U.S. veteran. Inquiries regarding non-discrimination policies may be directed to Office of Equal Opportunity, Title IX/ADA Coordinator, and Affirmative Action Officer, 3350 Beardshear Hall, Ames, Iowa 50011, 515-294-7612, email eooffice@iastate.edu.

Notice

The contents of this report reflect the views of the authors, who are responsible for the facts and the accuracy of the information presented herein. The opinions, findings and conclusions expressed in this publication are those of the authors and not necessarily those of the sponsors.

This document is disseminated under the sponsorship of the U.S. DOT UTC program in the interest of information exchange. The U.S. Government assumes no liability for the use of the information contained in this document. This report does not constitute a standard, specification, or regulation.

The U.S. Government does not endorse products or manufacturers. If trademarks or manufacturers' names appear in this report, it is only because they are considered essential to the objective of the document.

Quality Assurance Statement

The Federal Highway Administration (FHWA) provides high-quality information to serve Government, industry, and the public in a manner that promotes public understanding. Standards and policies are used to ensure and maximize the quality, objectivity, utility, and integrity of its information. The FHWA periodically reviews quality issues and adjusts its programs and processes to ensure continuous quality improvement.

Technical Report Documentation Page

1. Report No.	2. Government Accession No.	3. Recipient's Catalog No.

4. Title and Subtitle	5. Report Date
Machine-Vision-Based Roadway Health Monitoring and Assessment: Development of a Shape-Based Pavement-Crack-Detection Approach	January 2016
	6. Performing Organization Code

7. Author(s)	8. Performing Organization Report No.
Teng Wang, Kasthurirangan Gopalakrishnan, Arun Somani, Omar Smadi, and Halil Ceylan	

9. Performing Organization Name and Address	10. Work Unit No. (TRAIS)
Institute for Transportation Iowa State University 2711 South Loop Drive, Suite 4700 Ames, IA 50010-8664	**11. Contract or Grant No.** Part of DTRT13-G-UTC37

12. Sponsoring Organization Name and Address		13. Type of Report and Period Covered
Midwest Transportation Center 2711 S. Loop Drive, Suite 4700 Ames, IA 50010-8664	U.S. Department of Transportation Office of the Assistant Secretary for Research and Technology 1200 New Jersey Avenue, SE Washington, DC 20590	Final Report **14. Sponsoring Agency Code**

15. Supplementary Notes

Visit www.intrans.iastate.edu for color pdfs of this and other research reports.

16. Abstract

State highway agencies (SHAs) routinely employ semi-automated and automated image-based methods for network-level pavement-cracking data collection, and there are different types of pavement-cracking data collected by SHAs for reporting and management purposes.

The main objective of this proof-of-concept research was to develop a shape-based pavement-crack-detection approach for the reliable detection and classification of cracks from acquired two-dimensional (2D) concrete and asphalt pavement surface images.

The developed pavement-crack-detection algorithm consists of four stages: local filtering, maximum component extraction, polynomial fitting of possible crack pixels, and shape metric computation and filtering. After completing the crack-detection process, the width of each crack segment is computed to classify the cracks.

In order to verify the developed crack-detection approach, a series of experiments was conducted on real pavement images without and with cracks at different severities. The developed shape-based pavement crack detection algorithm was able to detect cracks at different severities from both asphalt and concrete pavement images. Further, the developed algorithm was able to compute crack widths from the images for crack classification and reporting purposes.

Additional research is needed to improve the robustness and accuracy of the developed approach in the presence of anomalies and other surface irregularities.

17. Key Words	18. Distribution Statement
asphalt pavement condition—concrete pavement condition—image-based crack detection—pavement condition monitoring—pavement cracking data—shape-based algorithm	No restrictions.

19. Security Classification (of this report)	20. Security Classification (of this page)	21. No. of Pages	22. Price
Unclassified.	Unclassified.	46	NA

Form DOT F 1700.7 (8-72) **Reproduction of completed page authorized**

MACHINE-VISION-BASED ROADWAY HEALTH MONITORING AND ASSESSMENT: DEVELOPMENT OF A SHAPE-BASED PAVEMENT-CRACK-DETECTION APPROACH

Final Report
January 2016

Principal Investigator
Kasthurirangan Gopalakrishnan, Research Associate Professor
Institute for Transportation, Iowa State University

Co-Principal Investigators
Omar Smadi, Director
Roadway Infrastructure Management and Operations Systems (RIMOS)
Institute for Transportation, Iowa State University

Arun Somani, Professor
Department of Electrical and Computer Engineering, Iowa State University

Halil Ceylan, Director
Program for Sustainable Pavement Engineering and Research (PROSPER)
Institute for Transportation, Iowa State University

Research Assistant
Teng Wang

Authors
Teng Wang, Kasthurirangan Gopalakrishnan, Arun Somani, Omar Smadi, and Halil Ceylan

Sponsored by
Midwest Transportation Center, and
U.S. Department of Transportation
Office of the Assistant Secretary for Research and Technology

A report from
Institute for Transportation
Iowa State University
2711 South Loop Drive, Suite 4700
Ames, IA 50010-8664
Phone: 515-294-8103 / Fax: 515-294-0467
www.intrans.iastate.edu

TABLE OF CONTENTS

LIST OF FIGURES

LIST OF TABLES

ACKNOWLEDGMENTS

The authors would like to thank the the Midwest Transportation Center and the U.S. Department of Transportation Office of the Assistant Secretary for Research and Technology for sponsoring this research. Special thanks to Qiuqi Cai (undergraduate researcher) for contributing to the state-of-the-art review on automatic detection of pavement cracks.

EXECUTIVE SUMMARY

State highway agencies routinely employ highway-speed-data-collection vehicles equipped with downward-looking digital cameras for the collection of network-level pavement images. These digital pavement images are then processed using proprietary semi-automated or fully automated image processing algorithms to identify pavement cracking information for reporting and use in pavement management systems for agency decision making regarding pavement preservation and rehabilitation.

Advancements are still being made in the development of accurate and reliable image-based pavement crack detection and classification algorithms. There is a need for the development of automated, low-cost crack-detection algorithms that could be implemented by highway agencies for cost-effective and continuous roadway health monitoring and management.

The main objective of this proof-of-concept research was to develop a shape-based pavement-crack-detection approach for the reliable detection and classification of cracks from acquired two-dimensional (2D) concrete and asphalt pavement images. Concrete and asphalt pavement JPEG images acquired through the 2D area-scanning digital-imaging method (dimensions of 3,072 by 2,048 pixels) were used for the analysis.

The developed pavement-crack-detection approach takes advantage of the spatial distribution of crack pixels and works on each pavement image block of 75 by 75 pixels. The overall crack-detection algorithm consists of four stages: local filtering, maximum component extraction, polynomial fitting of possible crack pixels, and shape metric computation and filtering. After completing the crack detection process, the width of each crack segment is computed to classify the cracks.

In order to verify the developed crack-detection approach, a series of experiments was conducted on real pavement images without and with cracks at different severities. The developed shape-based pavement-crack-detection algorithm was able to detect cracks at different severities from both asphalt and concrete pavement images. Further, the developed algorithm was able to compute crack widths from the images for crack classification and reporting purposes.

Additional research is needed to improve the robustness and accuracy of the developed approach in the presence of anomalies and other surface irregularities.

INTRODUCTION

Problem Statement

Pavement management can be traced as early as the ancient Roman Empire, but pavement management using computer systems began during the 1970s. Advances in pavement health monitoring technologies and pavement management systems (PMSs) have helped transportation agencies make discoveries about the best practices for preventive maintenance and pavement management.

Highway surfaces are typically designed for 15 to 20 years of normal deterioration, assuming that routine maintenance functions (such as crack sealing and pothole patching) are carried out. Efficient health monitoring strategies for bridges and pavements can aid engineers in identifying developing distresses and scheduling maintenance early.

Highway and pavement health monitoring techniques can broadly be classified under four major categories: deflection-based, image-based, wave propagation-based, and in situ sensing-based. Each one addresses the health-monitoring objective from a different perspective and foundation.

Image-based health monitoring methods have a history of more than 30 years, and they have primarily been focused on pavement surface cracking, because that is one of the pavement distresses that can be easily captured through imaging. What began as windshield or manual surveys evolved into capturing analog photographs or videotapes, which were then processed to extract pavement-cracking information.

The current state-of-the-practice is to acquire two-dimensional (2D) digital images of pavements using high-speed cameras mounted on a specialized data-collection van moving at highway traffic speeds. Once the high-resolution digital images of the pavement surfaces are obtained, they are processed through a compression subsystem to achieve size reduction without loss of quality before they are stored. The images are then processed using various algorithms to extract cracking information and summary statistics, which are then recorded in the surface distress database (and can be linked to a PMS).

Advancements are still being made in the development of accurate and reliable image-based pavement-crack-detection and classification algorithms. There is a need for the development of automated, low-cost crack detection algorithms that can be implemented by highway agencies for cost-effective and continuous roadway health monitoring and management.

Research Objective and Approach

The objective of this proof-of-concept research project was to develop a shape-based pavement-crack-detection approach for the reliable detection and classification of cracks from acquired 2D pavement images.

The developed approach takes advantage of the spatial distribution of crack pixels and works on each pavement image block of 75 by 75 pixels. The overall crack detection algorithm consists of four stages: local filtering, maximum component extraction, polynomial fitting of possible crack pixels, and shape metric computation and filtering. After completing the crack-detection process, the width of each crack segment is computed to classify the cracks.

IMAGE-BASED PAVEMENT CRACKING DATA COLLECTION AND PROCESSING: A BRIEF REVIEW

Existing Pavement Cracking Data Collection Practices

Many state and local agencies employ highway-speed data-collection vehicles to collect pavement images, which are then processed using proprietary image processing algorithms to classify cracking type, extent, and severity. The Federal Highway Administration (FHWA) Long-Term Pavement Performance Program (LTPP) developed the Distress Identification Manual, which provides a consistent and uniform method to collect and report pavement distress data for the LTPP.

Most state highway agencies (SHAs) have their own distress identification/survey manuals, some of which are listed below, that have been modified from the LTPP distress identification manual to fit each agency's data collection needs for pavement management and design:

- Colorado (2004): *Colorado DOT Distress Manual for HMA and PCC Pavements*
- Minnesota (2003): *Mn/DOT Distress Identification Manual*
- Nebraska (2012): *Surface Distress Survey Manual*
- Oregon (2010): *Pavement Distress Survey Manual*
- South Dakota (2009): *SDDOT's Enhanced Pavement Management System: Visual Distress Survey Manual*
- Texas (2010): *Texas DOT Pavement Management Information System: Rater's Manual*
- Utah (2003): *Utah DOT Distress Manual*
- Virginia (2012): *A Guide to Evaluating Pavement Distress Through The Use of Digital Images*

According to National Cooperative Highway Research Program (NCHRP) Synthesis 401, *Quality Management of Pavement Condition Data Collection*, transverse cracking and fatigue cracking are among the distresses for which data are most commonly collected by highway agencies, as shown in Figure 1 (Flintsch and McGhee 2009).

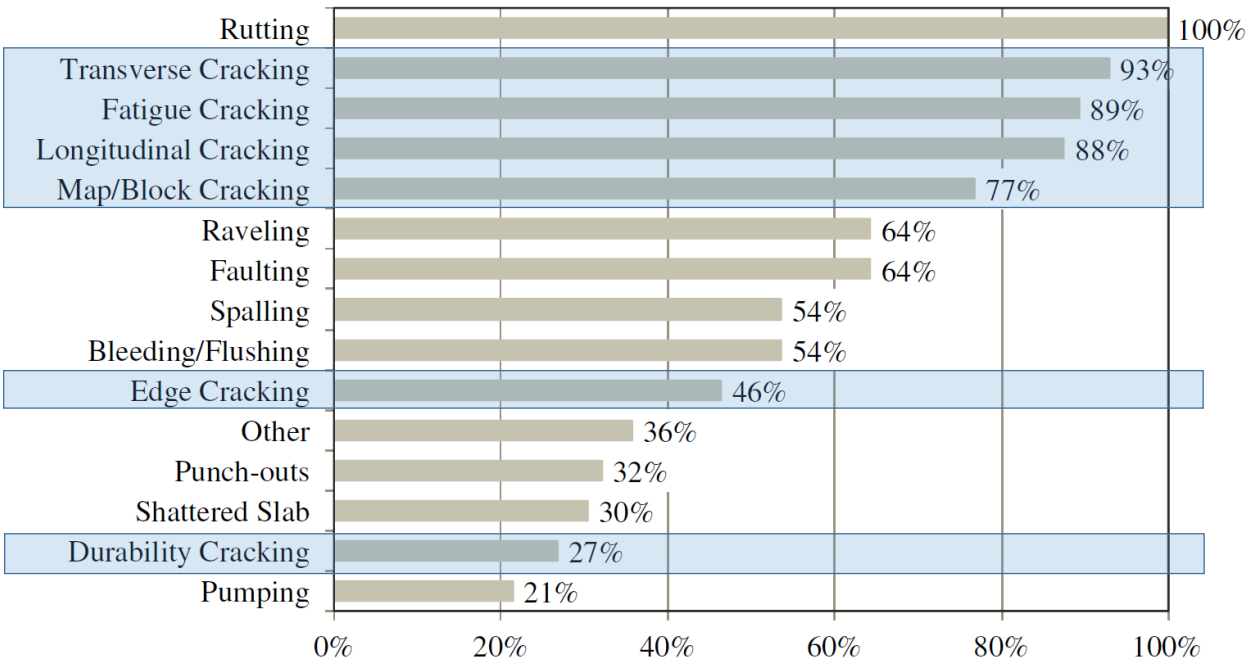

Flintsch and McGhee 2009

Figure 1. Different types of pavement cracking data collected by state highway agencies

Based on a survey of pavement distress definitions used by state departments of transportation (DOTs), NCHRP Synthesis 457, *Implementation of the AASHTO Mechanistic-Empirical Pavement Design Guide and Software*, indicated that most responding agencies had their asphalt concrete (AC) alligator cracking (36 agencies) and jointed plain concrete pavement (JPCP) transverse cracking (35 agencies) data collection procedures consistent with the procedures in the LTPP Distress Identification Manual (Miller and Bellinger 2003), while longitudinal cracking, thermal cracking, and reflective cracking data collection procedures for AC-surfaced pavements were often not consistent with the LTPP data collection procedures (Pierce and McGovern 2014).

As of 2012, more than 35 state highway agencies employed semi-automated and automated image-based methods for network-level pavement cracking data collection (Vavrik et al. 2013). The various sources of variability in pavement cracking data collection and processing for automated, semi-automated, and manual methods are summarized in Figure 2.

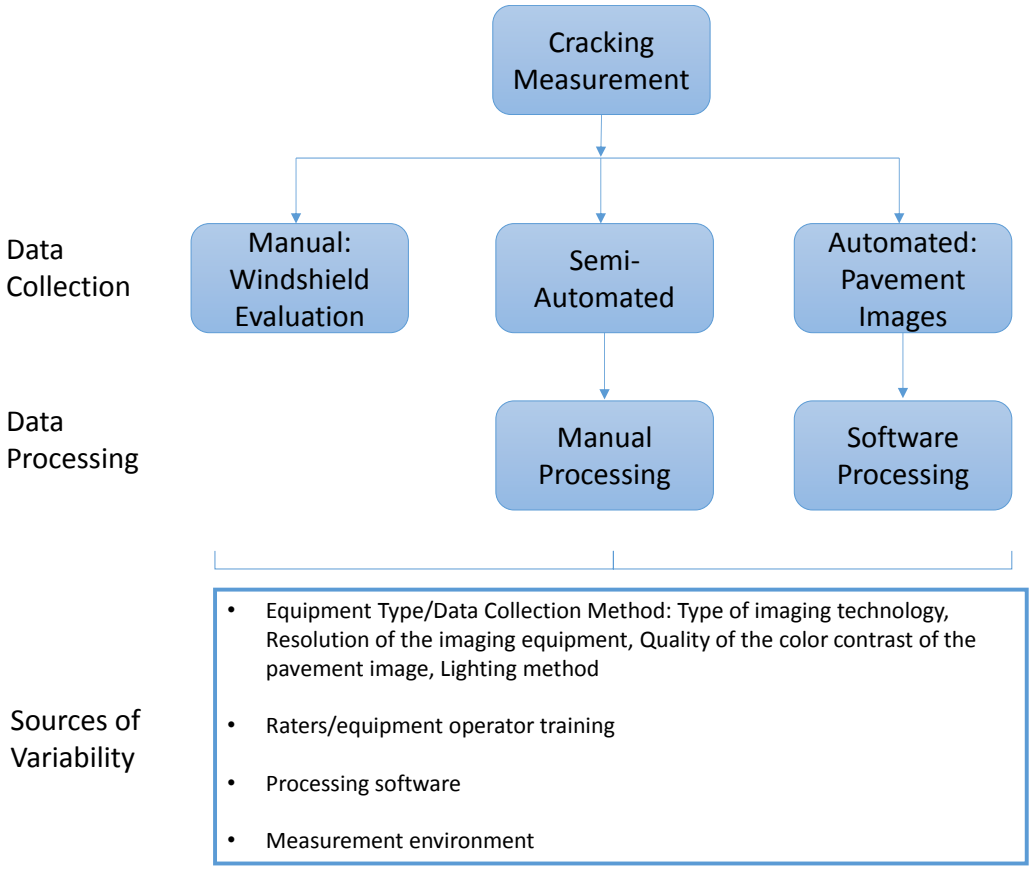

Flintsch and McGhee 2009, McNeil and Humplick 1991

Figure 2. Sources of variability in pavement cracking data collection and processing

Studies have highlighted that a noticeable bias exists in automated crack detection methods toward detecting high-severity cracking than low-severity cracking because high-severity cracking is in general, more readily identifiable than low- or medium-severity cracking (McQueen and Timm 2005, Flintsch and McGhee 2009).

NCHRP Synthesis 334, *Automated Pavement Distress Collection Techniques*, documents highway agency practices with regard to the automated collection and processing of pavement condition data techniques typically used in network-level pavement management. Factors that could potentially contribute to variability in automated pavement cracking data collection and processing practices adopted by various highway agencies (based on a survey conducted in 2003) are summarized below (McGhee 2004):

- Automated cracking data collection: agency, contract
- Automated cracking data processing: agency, contract
- Image capture: analog, digital, laser
- Protocol use: American Association of State Highway and Transportation Officials (AASHTO), LTPP, other
- Monitoring frequency (years): 1, 2, 3

- Reporting intervals: 100–300 m, 10–50 m, segment, other
- Linear reference methods: mile post, latitude-longitude, link-node, log mile, other

The various pavement cracking types and summary descriptions from the LTPP distress identification manual and AASHTO PP 67-10, the two major protocols used by highway agencies, are summarized in Table 1 and Table 2, respectively. A variety of pavement cracking data is desired by the SHAs, not only for their asset/pavement management activities, but also for FHWA's Highway Performance Monitoring System (HPMS) reporting requirements and for evaluating and calibrating the AASHTOWare Pavement ME Design software (currently being implemented by several SHAs). Recent changes in HPMS requirements demand that the state DOTs collect the following detailed cracking data (Vavrik et al. 2013):

- AC pavements: fatigue cracking (percent area), transverse cracking (ft/mi)
- Portland cement concrete (PCC) pavements: cracking (percent area); longitudinal cracking for continuously reinforced concrete pavement (CRCP)
- AC/PCC pavements: fatigue cracking (percent area), transverse reflective cracking (ft/mi)

Table 1. Various pavement cracking types, descriptions, and defined severity levels summarized in the LTPP distress identification manual

Pavement Type	Cracking Type (Unit of Measure)	Summary Description	Defined Severity Levels
AC-surfaced	Fatigue Cracking (m^2 or ft^2)	Series of interconnected cracks in areas subjected to repeated traffic loadings (wheel paths).	Yes
	Block Cracking (m^2 or ft^2)	Pattern of cracks that divides the pavement into approximately rectangular pieces.	Yes
	Edge Cracking (m or ft)	Crescent-shaped cracks adjacent to unpaved shoulder.	Yes
	Wheel Path Longitudinal Cracking (m or ft)	Cracks predominantly parallel to pavement centerline (wheel path)	Yes
	Non-Wheel Path Longitudinal Cracking (m or ft)	Cracks predominantly parallel to pavement centerline (non-wheel path)	Yes
	Transverse Reflection Cracking (reported as Transverse Cracking)	Transverse cracks in AC overlay surfaces that occur over joints in concrete pavements	N/A
	Longitudinal Reflection Cracking (reported as Longitudinal Cracking)	Longitudinal cracks in AC overlay surfaces that occur over joints in concrete pavements	N/A
	Transverse Cracking (No., m or ft)	Cracks that are predominantly perpendicular to pavement centerline	Yes
PCC-surfaced	Corner Breaks (No.)	A portion of the slab separated by a crack intersecting the adjacent transverse and longitudinal joints at 45-deg	Yes
	"D" cracking (No., m^2 or ft^2)	Closely spaced crescent-shaped hairline cracking pattern	Yes
	Longitudinal Cracking (m or ft)	Cracks that are predominantly parallel to the pavement centerline	Yes
	Transverse Cracking (No., m or ft)	Cracks that are predominantly perpendicular to the pavement centerline	Yes
	Map Cracking (No., m^2 or ft^2)	A series of cracks that extend only into the upper surface of the slab	N/A

Miller and Bellinger 2003

Table 2. Various pavement cracking types, descriptions, and defined severity levels summarized in AASHTO PP 67-10

Pavement Type	Cracking Type (Unit of Measure)	Summary Description	Defined Severity Levels
AC-surfaced	Longitudinal Crack (m or ft)	A crack at least 0.3 m long and with a crack orientation between +10 and –10 deg.	Yes
	Transverse Crack (m or ft)	A crack at least 0.3 m long and with a crack orientation between 80 and 100 deg.	Yes
	Pattern Crack (m or ft)	A crack that is part of a network of cracks that form an identifiable grouping of shapes	Yes

Pavement Crack Detection and Classification

TR Circular No. E-C156, *Automated Imaging Technologies for Pavement Distress Surveys*, summarized the current state-of-the-art in the acquisition and processing of pavement surface images (Wang and Smadi 2011). In recent years, several advances have been made in image collection technology, equipment hardware and software, decoding and extraction methods, etc. A number of projects sponsored by SHAs, the National Cooperative Highway Research Program (NCHRP), and the FHWA have been initiated and completed with the objective of automating and improving image-based pavement distress detection and classification. Under High-Speed Rail IDEA Project 49, Ahuja and Barkan (2007) employed machine vision analysis by imaging both visible and infrared spectra of railroad equipment undercarriage for addressing incipient failure detection. A prototype of the machine vision inspection system was developed and tested at a passenger car service and inspection facility. Elkrry and Anderson (2013) provided a comprehensive summary of the network-level and project-level non-invasive imaging technologies applicable to pavement assessment. An Iowa DOT project (Neubauer and Todsen 2013) is investigating the use of acoustic imaging equipment to inspect bridge substructural elements.

More recently, studies have been exploring the potential for using three-dimensional (3D) laser imaging technology for pavement distress surveys. Wang and Li (2014) proposed the use of 3D laser imaging for pavement surface data collection on the Oklahoma DOT Interstate network, including longitudinal profile, transverse profile, macro-texture, cracking, and various surface defects. Under a project sponsored by the Southern Plains Transportation Center, Wang (2014) is investigating the use of 1 mm 3D laser imaging (PaveVision3D system) for pavement surface characterization (mean texture depth, mean profile depth, etc.) related to pavement safety. An ongoing Florida DOT–sponsored research project (Roque 2014) is investigating the application of imaging techniques to evaluate the polishing characteristics of aggregates. An Ohio DOT/FHWA–sponsored research project (Wei et al. 2014) is currently investigating the use of a

nonintrusive side-of-the-road camera to develop a rapid video-based vehicle identification (RVIS) system.

A summary of selected studies in recent years that have focused on improving image-based pavement distress detection methods is provided in Table 3.

Table 3. Summary of selected recent studies that have focused on the improvement of automated pavement crack identification and classification

No.	Reference	Innovation
1	Sun and Qiu (2007)	Use of multi-scale morphologic edge detection method for automatic identification of cracks
2	Oliveria and Correia (2009)	Use of anisotropy measure and multi-layer perceptron neural networks to classify cracks
3	Lairong et al. (2009)	Use of support vector machine (SVM) to design pavement crack classifier
4	Zhang et al. (2009)	Use of Wiener filter to improve pavement crack identification accuracy
5	Liang and Sun (2010)	Use of wavelet technology for edge detection of cracks from pavement surface images
6	Zou et al. (2012)	Use of geodesic shadow-removal algorithm and recursive tree-edge pruning to detect cracks from asphalt pavement images
7	Adarkwa and Attoh-Okine (2013)	Use of tensor decomposition in pavement crack classification
8	Peng et al. (2014)	Automatic crack detection by multi-seeding fusion on 1 mm resolution 3D pavement images

DEVELOPMENT OF A SHAPE-BASED PAVEMENT CRACK DETECTION APPROACH

We propose a shape-based pavement crack detection approach, taking advantage of the spatial distribution of crack pixels. This approach works on each pavement image block of size 75 by 75 pixels and consists of four stages:

- Local filtering
- Maximum component extraction
- Polynomial fitting of possible crack pixels
- Shape metric computation and filtering

Local Filtering

Considering the fact that crack pixels have relatively lower intensity values compared to non-crack pixels in one pavement image, we first design a filter to remove non-crack pixels for each pavement block, $RawBlock^{(i)}$. The filter is defined as follows:

$$\boldsymbol{FilterBlock}^{\{(\boldsymbol{i})\}(\boldsymbol{x})} = \begin{cases} 1, if\ \boldsymbol{RawBlock}^{(\boldsymbol{i})}(\boldsymbol{x}) < \boldsymbol{f} * \boldsymbol{\mu}^{(\boldsymbol{i})} \\ 0, else \end{cases} \quad (1)$$

where $RawBlock^{(i)}(x)$ and $FilterBlock^{(i)}(x)$ represent the image intensity at position x in input pavement block, $RawBlock^{(i)}$, and output pavement block, $FilterBlock^{(i)}$, respectively; $^{(i)}$ is the mean intensity value of input block $RawBlock^{(i)}$; and parameter f is empirically set as 0.8 based on histogram analysis.

Output $FilterBlock^{(i)}$ is a binary image, where white and black pixels correspond to possible crack pixels and non-crack pixels, respectively. We give an example to show the performance of filtering in Figure 3. We make the observation from Figure 3 that the local filter has the capability to extract crack pixels, although it introduces some noise from pavement textures.

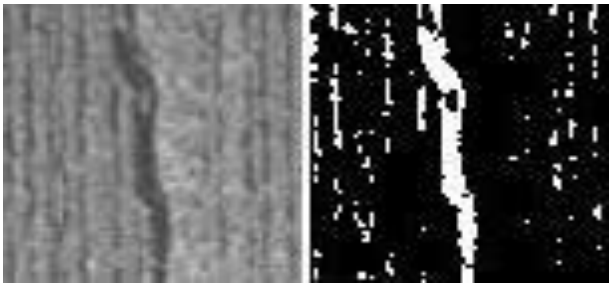

Figure 3. Example of local filtering to remove non-crack pixels: Input $RawBlock^{(i)}$ (left) and Output $FilterBlock^{(i)}$ (right)

Major Component Extraction

Because the local filter introduces some noise from pavement texture when extracting crack pixels, we need to develop a major component extraction approach to refine crack pixels from all possible crack pixels. Our major component extraction process consists of two steps: (1) minor component removal and (2) maximum component extraction.

- Minor Component Removal: we employ the MATLAB function *bwareaopen()* to remove minor components. The details are given as follows:

  $MajorBlock^{(i)}$ = bwareaopen($FilterBlock^{(i)}$; 10)

  This MATLAB command aims to remove minor connected components whose sizes are smaller than 10 pixels. We test the minor component removal approach on the filtered binary crack block as shown in Figure 4 (left) and display the output block in Figure 4 (right).

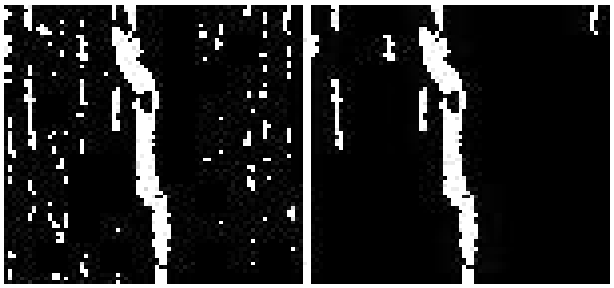

Figure 4. An example of minor component removal: Input *FilterBlock*$^{(i)}$ (left) and Output *MajorBlock*$^{(i)}$ (right)

- Maximum Component Extraction: We employ the MATLAB function *bwconncomp(MajorBlock*$^{(i)}$*)* to get all connected components in crack block, *MajorBlock*$^{(i)}$, and remove all but the component with the maximum area. We employ *MaxBlock*$^{(i)}$ to denote the final output image containing only the maximum component. We test the whole process of maximum component extraction on a set of raw pavement blocks and display one typical example in Figure 5.

Figure 5. Example of maximum component extraction: Input *MajorBlock*$^{(i}$ (left) and Output *MaxBlock*$^{(i)}$ (right)

We make the following observations from the experiment results:

- **Case 1: Continuous Pavement Crack.** In this case, the output maximum component has the capability to accurately track the whole pavement crack. The width of the pavement cracks in medium- or high-severity cracking is usually larger than 2 pixels. For those cracks wider than 2 pixels, the size of the maximum components is higher than 150 pixels with a probability as high as 99.99%. An example of a continuous crack of medium severity is given in Figure 6 (far left). We test the maximum component extraction approach on the crack block and display the result in Figure 6 (far right). The maximum component overlaps with the continuous pavement crack very well, and the size of the crack component is 196 pixels.

Figure 6. Example of continuous pavement crack (from left to right): raw crack block, local filtering, minor removal, and maximum extraction

- **Case 2: Noncontinuous Pavement Crack.** Due to interruptions, the maximum component from the extraction process corresponds to the major part of the noncontinuous crack in this scenario. The size of the maximum component depends on the crack width, number of interruptions, and the locations of the interruptions. For a noncontinuous crack at low or medium severity, the size of its maximum component will be between 50 and 150 pixels with a high probability. An example of a noncontinuous crack at medium severity is given in Figure 7 (far left). We present the maximum component from the crack block in Figure 7 (far right). There are four interruptions in the pavement crack, and the maximum component is from the top part (i.e., the largest one). The size of the component is equal to 121 pixels.

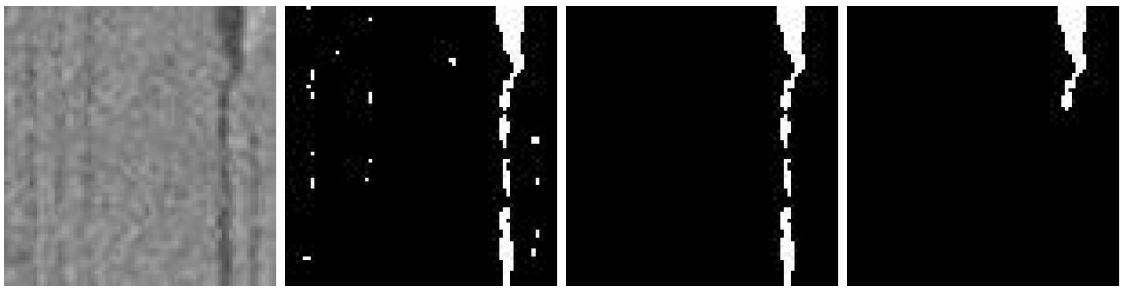

Figure 7. Example of noncontinuous pavement crack at medium severity (from left to right): raw crack block, local filtering, minor removal, and maximum extraction

- **Case 3: Non-Crack Pavement Block with Strong Longitudinal Tined Texture.** The sizes of the maximum components from non-crack pavement blocks with a strong longitudinal

tined texture are almost in the same range as those from noncontinuous cracks at low and medium severity, i.e., lying between 50 and 150 pixels with a probability as high as 90%. Figure 8 (far left) shows an example of a non-crack pavement block with a strong longitudinal tined texture. We test the maximum component extraction process on the block and display the maximum component in Figure 8 (far right), whose size is equal to 130 pixels.

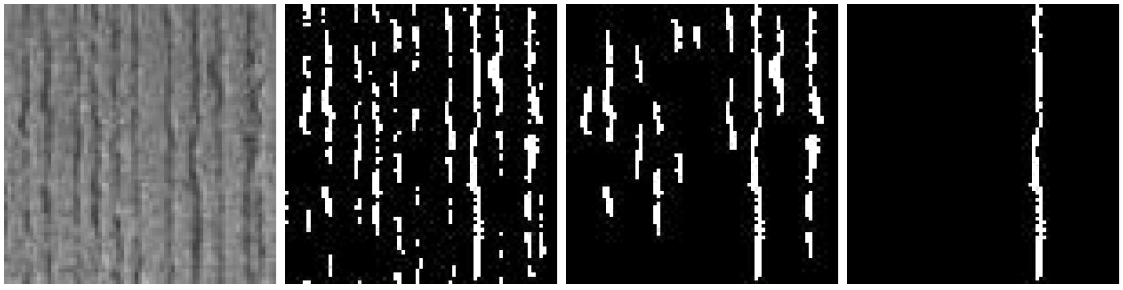

Figure 8. Example of non-crack pavement block with strong longitudinal tined texture (from left to right): raw pavement block, local filtering, minor removal, and maximum extraction

- **Case 4: Non-Crack Pavement Block with Light Longitudinal Tined Texture.** The sizes of the maximum components from non-crack pavement blocks with a smooth texture are smaller than 50 pixels with a probability as high as 99%. Figure 9 (far left) shows an example of a non-crack pavement block with a light longitudinal tined texture. We test the maximum component extraction process on the block and display the maximum component in Figure 9 (far right). The size of the component is equal to 18 pixels.

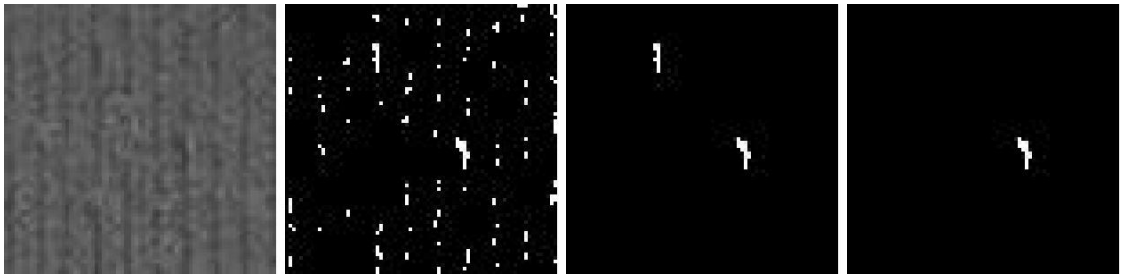

Figure 9. Example of non-crack pavement block with light longitudinal tined texture (from left to right): raw pavement block, local filtering, minor removal, and maximum extraction

Based on the above discussion, we conclude that when pavement cracks at medium or low severity are noncontinuous, the whole crack extraction process will produce maximum components of small sizes, even smaller than those from non-crack pavement blocks with a strong tined texture. Therefore, it is not proper to detect pavement cracks based on the area of the maximum component alone. As a result, we need to develop a new metric to distinguish crack blocks from non-crack blocks. By comparing Figure 7 to Figure 8, we notice that one major difference between noncontinuous crack and non-crack blocks with strong tined textures is the spatial distribution (i.e., shape) of possible crack pixels in binary block *MajorIm*, i.e., the output

of the minor removal process. However, non-crack blocks with a light tined texture differ from crack blocks mainly in the size of the maximum component in binary block *MaxIm*. We first make the following modification to the definition of the maximum component:

For each pavement block $RawBlock^{(i)}$,

- Case 1: $\boldsymbol{Size(MaxBlock^{(i)}) >= T1}$ (i.e., continuous crack block),

  No changes.

- Case 2: $\boldsymbol{Size(MaxBlock^{(i)}) >= T2 \&\& Size(MaxBlock^{(i)}) < T1}$ (i.e., noncontinuous crack block or non-crack pavement block with a strong tined texture),

  $\boldsymbol{MaxBlock^{(i)} = MajorBlock^{(i)}}$**.**

- Case 3: $\boldsymbol{Size(MaxBlock^{(i)}) < T2}$ (i.e., pavement block with a light tined texture),

  $\boldsymbol{MaxBlock^{(i)} = FilterBlock^{(i)}}$**.**

where *T1* and *T2* are empirically set to 150 and 50, respectively. Operations in Case 2 and Case 3 are called maximum expansion. Then, the difference between crack blocks and non-crack blocks can be simplified as the spatial distribution of all possible crack pixels in binary image $MaxBlock^{(i)}$. In the following subsection, we aim to develop a metric to measure the closeness of possible crack pixels in binary image $MaxBlock^{(i)}$.

Polynomial Fitting

With maximum component $MaxBlock^{(i)}$ available, we fit a polynomial curve to all possible crack pixels and compute the average fitting error. Polynomial fitting and fitting error computation are achieved by MATLAB functions *polyfit()* and *polyval()*, respectively. Because we do not know the orientation of the pavement cracks in advance, we fit cracks in both the horizontal and vertical directions in order to handle the scenarios of straightly oriented horizontal and vertical cracks. Then, we select one minimizing fitting error as the final fitting curve. Details are given as follows:

$$polyfuncH = polyfit(CX, CY, 3) \tag{2}$$

$$polyfuncY = polyfit(CY, CX, 3) \tag{3}$$

where $CX = \{cx_1; cx_2; cx_3; \ldots; cx_N\}$, and $CY = \{cy_1; cy_2; cy_3; \ldots; cy_N\}$ are the position vectors of crack pixels in the X and Y directions, respectively; *polyfuncH* and *polyfuncV* are the returned polynomial fitting functions in the horizontal and vertical directions, respectively; and *N* is the

total number of possible crack pixels in maximum component *MaxBlock*$^{(i)}$. In this project, we employ a third-order polynomial curve to fit the pavement cracks. With the polynomial functions available, we compute the fitting error, *AveErr*, as follows:

$$c\hat{y}_k = \text{polyval}(\text{polyfuncH};\ cx_k);\ \text{where } k \in 1, 2, \dots, N \tag{4}$$

$$c\hat{x}_k = \text{polyval}(\text{polyfuncV};\ cy_k);\ \text{where } k \in 1, 2, \dots, N \tag{5}$$

$$AveErr^H = \frac{\sum_{k=1}^{N}((c\widehat{y}_k - cy_k)^2)}{N} \tag{6}$$

$$AveErr^V = \frac{\sum_{k=1}^{N}((c\widehat{x}_k - cx_k)^2)}{N} \tag{7}$$

$$AveErr = \min\{AveErr^H, AveErr^V\} \tag{8}$$

An example of polynomial fitting is shown in Figure 10. Figure 10 (left) is the binary crack block after maximum component extraction. We test both vertical and horizontal polynomial fitting on the crack block and display the fitting results in Figure 10 (center and right).

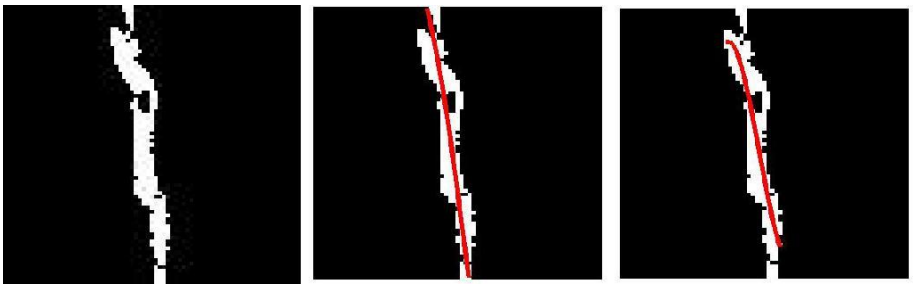

Figure 10. Example of polynomial fitting of crack pixels: MaxBlock$^{(i)}$ (left), vertical fitting (center), and horizontal fitting (right)

The average polynomial fitting errors in the vertical and horizontal directions are equal to 3.6303 and 120.8035, respectively. Therefore, we fit the crack in the vertical direction, and the final average fitting error of the crack block is equal to 3.6303.

Shape Metric Computation and Threshold Filtering

With the average polynomial fitting error available, we employ it to define a shape metric (SM) measuring the closeness of pixels in a maximum component as follows:

$$SM = AveErr/N \tag{9}$$

It is worth mentioning that the shape metric has the following features:

- For an almost solid component, the shape metric increases with its width, as shown in Figure 11 (right). The details involved in the development of this chart are as follows. For each width value, *W*, we create a vertical pavement crack lying in the center of the block. The horizontal width for each *y* follows the uniform distribution between $0.5 \times W$ and W to mimic the true shapes of the cracks. An example of a 25 pixel wide crack via simulation is shown in Figure 11 (left). Because size of the pavement block is set to be 75 by 75 pixels, the maximum shape metric value is equal to about 0.007.

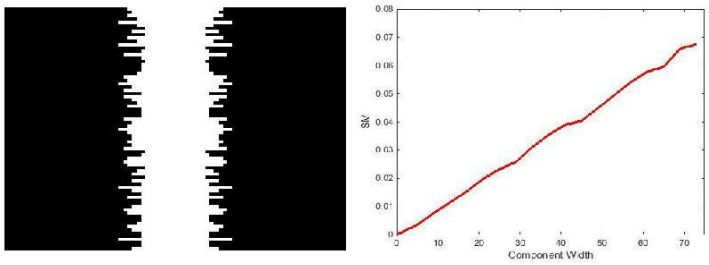

Figure 11. Relation between crack width and shape metric (SM): 25 pixel wide crack (left) and relation chart (right)

- For an unconnected component from the maximum expansion operation, the value of the shape metric will be relatively much higher due to the fact that the component pixels are widely distributed.

As a result, it is reasonable to detect pavement cracks based on the devised shape metric. A pavement block is considered to contain cracks if and only if its shape metric value is smaller than 0.08 (detection criterion).

In Figure 12 through Figure 15, we give some examples to show the shape metric values of crack and non-crack blocks. The shape metric value of the continuous crack block as shown in Figure 12 is 0.0112.

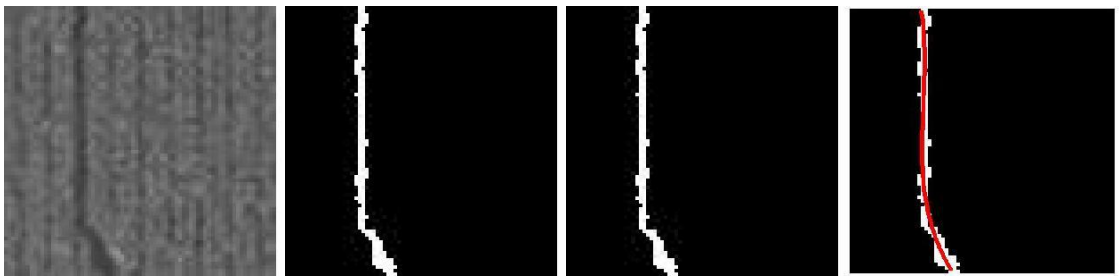

Figure 12. Example of polynomial fitting of continuous crack (left to right): raw crack block, maximum extraction, maximum expansion, and polynomial fitting

For the noncontinuous crack block shown in Figure 13 (far left), the shape metric value is equal to 0.0591.

Figure 13. Example of polynomial fitting of noncontinuous crack (left to right): raw crack block, maximum extraction, maximum expansion, and polynomial fitting

However, the shape metric values of the non-crack blocks shown in Figure 14 (far left) and Figure 15 (far left) are equal to 0.6235 and 1.2422, respectively.

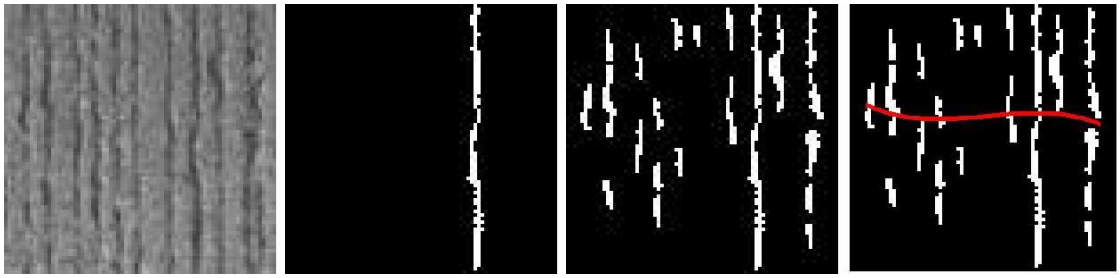

Figure 14. Example of polynomial fitting of non-crack block with strong tined texture (left to right): raw pavement block, maximum extraction, maximum expansion, and polynomial fitting

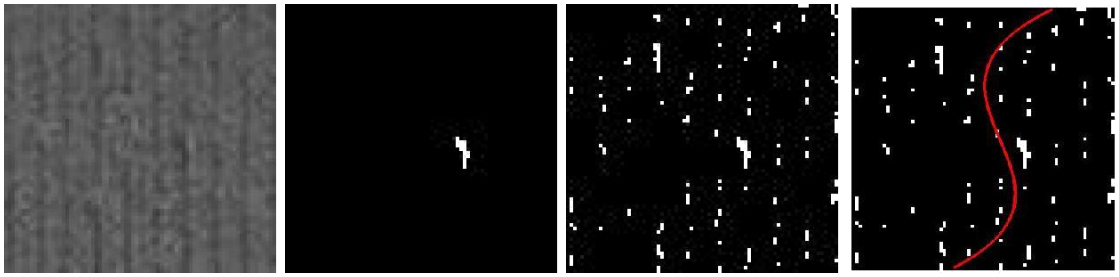

Figure 15. Example of polynomial fitting of non-crack block with light tined texture (left to right): raw pavement block, maximum extraction, maximum expansion, and polynomial fitting

Based on the detection criterion, the first two crack blocks will be classified as cracks, and the last two non-crack blocks will be classified as non-crack blocks, which satisfies our expectation.

Pavement Joint Detection

In this project, we focus only on detecting pavement cracks from acquired images and not detecting joints or road surface markings (such as those separating lanes or separating the

pavement from the shoulder). However, the acquired pavement images often include joints along with cracks. Because our proposed shape metric fails to distinguish cracks from joints, we design a pavement joint detection approach to remove joints before crack detection. One feature of pavement joints is that joint pixels are in straight lines. An efficient approach to detecting straight lines in an image is the Hough Transform. The details are as follows:

- Step1: Employ a Gaussian filter to remove noise from pavement image *rawPaveIm*.

  gausFilter = fspecial('gaussian', 15, 3.0),

  smoothPaveIm = imfilter(rawPaveIm, gausFilter, 'same'),

  where *fspecial* and *imfilter* are MATLB functions for creating a Gaussian filter and removing noise.

- Step 2: Employ the Canny method to extract edges from smoothed pavement image *smoothPaveIm*.

  edgePaveIm = edge(smoothPaveIm, 'Canny', 0.20),

  where *edge* is a MATLAB function used for identifying edges in an intensity image.

- Step 3: Use the Hough Transform to detect the existence of straight lines in binary image edgePaveIm.

  [H, T, R] = hough(edgePaveIm),

  *P = houghpeaks(H, 10, `threshold', ceil(0.10*max(H(:)))),*

  DLines = houghlines(edgePaveIm, T, R, P, `FillGap', 1500, 'MinLength', 100),

  where *hough*, *houghpeaks*, and *houghlines* are MATLAB functions to implement the Hough Transform and *Output Dlines* is the set of identified lines in the image.

Figure 16 shows an example of pavement divider detection. We overlap the detected pavement dividers in black with the raw pavement image in Figure 16 (far right) to facilitate observation.

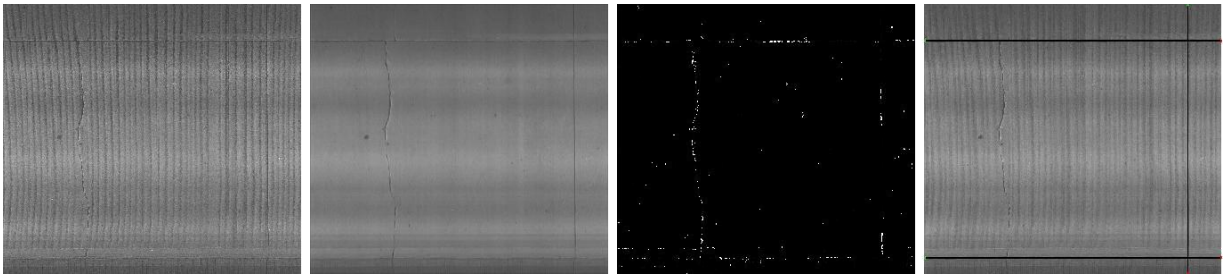

Figure 16. Example of pavement joint detection (left to right): raw pavement image, noise removal, edge detection, and joint detection

EXPERIMENTS IN PAVEMENT CRACK DETECTION USING THE PROPOSED APPROACH

We test our shape-based crack detection approach on different pavement datasets with various textures. The detection window is set to 75 by 75 pixels. For each pavement image, we move the detection window from left to right in a row and then move to the next row. Overlapping between neighboring detection windows in both the horizontal and vertical direction is set to 25 pixels.

Dataset 1: Pavement Images with Perfect Cracks

In this subsection, we test our shape-based crack detection approach on a set of pavement images containing perfect cracks at various severities. We present three raw pavement images in Figure 17 (left), Figure 18 (left), and Figure 19 (left).

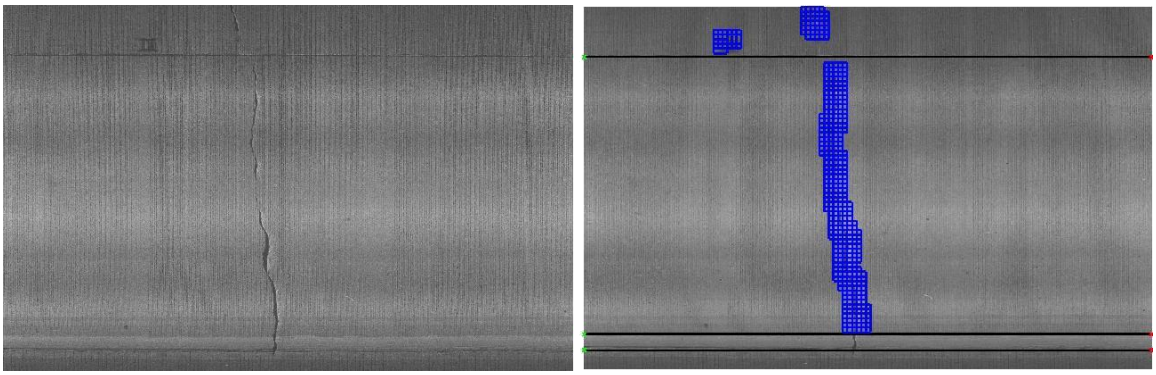

Figure 17. Example 1 of concrete crack at high severity: raw crack (left) and crack detection (right)

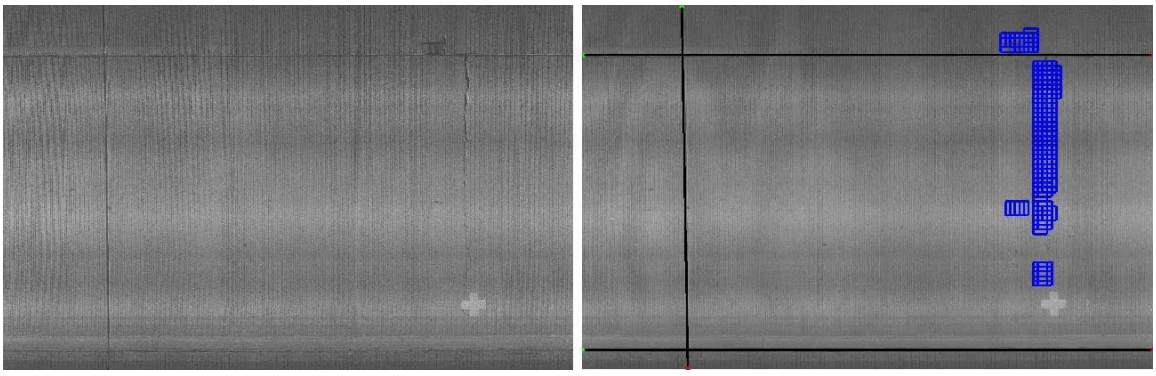

Figure 18. Example 2 of concrete crack at low severity: raw crack (left) and crack detection (right)

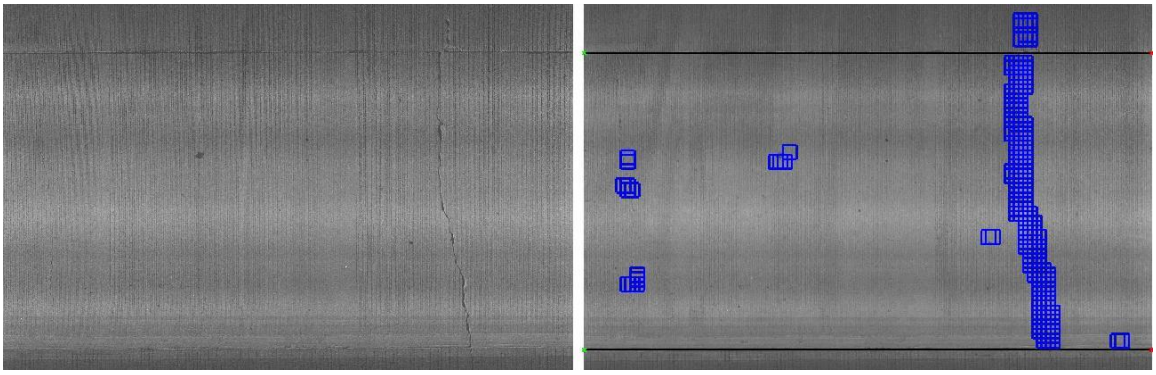

Figure 19. Example 3 of concrete cracks at high and low severities: raw crack (left) and crack detection (right)

Specifically, Figure 17 (left) contains a high-severity crack and an anomaly near the longitudinal joint. The pavement crack in Figure 18 (left) consists of different segments at various severities (i.e., the top, middle, and bottom segments are at high, medium, and low severity, respectively). Figure 19 (left) contains two cracks: the left one is at low severity and right one is at high severity. Shape-based crack detection results of the three pavement images are presented in Figure 17 (right), Figure 18 (right) and Figure 19 (right). We make the following observations from the detection results.

- In the first example (Figure 17), our approach successfully detects both the pavement crack and the anomaly near the longitudinal joint.

- In the second example (Figure 18), our approach successfully detects the pavement crack, missing part of crack segment in low severity.

- In the third example (Figure 19), our approach successfully detects both pavement cracks at high and low severity. In all three examples, our approach was also able to detect black patches whose size is larger than 50 pixels.

It is worth mentioning that the black lines in these figures represent horizontal and vertical dividers detected by the proposed pavement joint detection approach. Because we are only interested in cracks, not joints, we filter out all crack windows that intersect with pavement joints after the detection process.

Dataset 2: Concrete Cracks at Various Severities

In this subsection, we test our shape-based crack detection approach on a set of concrete crack images at various severity degrees to check the performance of our approach.

Detecting High-Severity Concrete Cracks

We give three examples of concrete cracks at high severity in the left-hand images in Figure 20, Figure 21, and Figure 22.

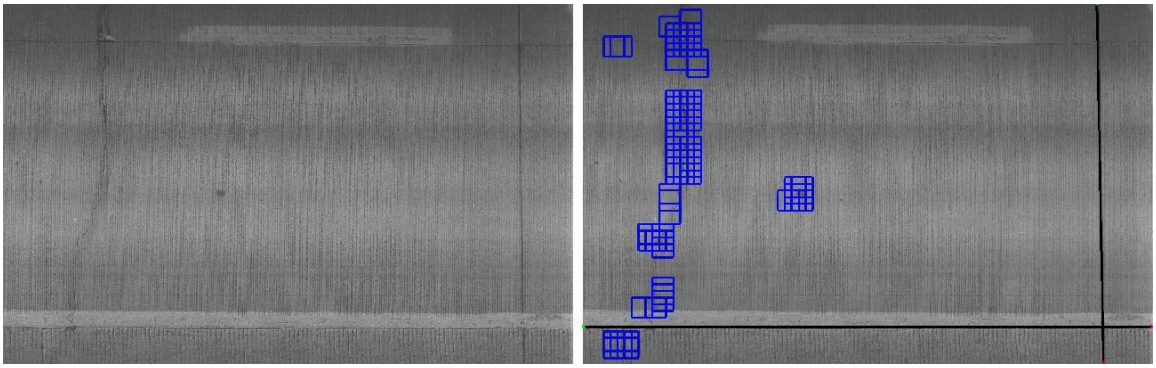

Figure 20. Example 1 of concrete crack at high severity: raw crack (left) and crack detection (right)

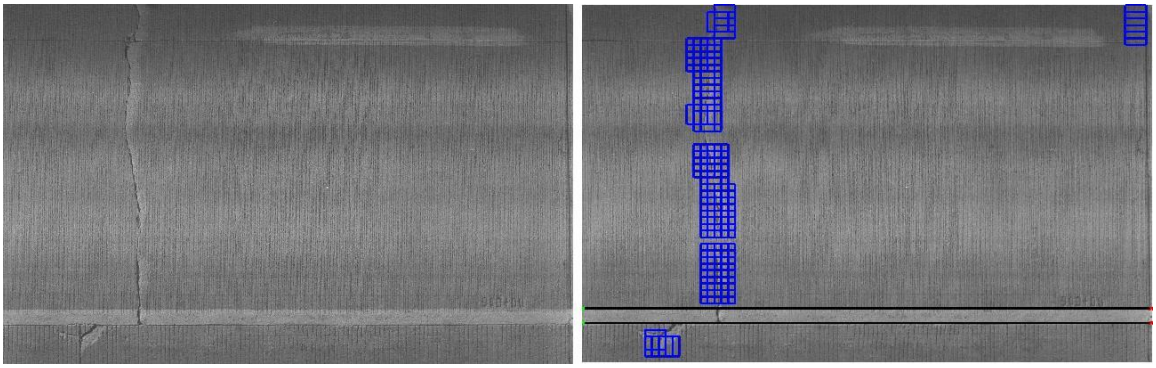

Figure 21. Example 2 of concrete crack at high severity: raw crack (left) and crack detection (right)

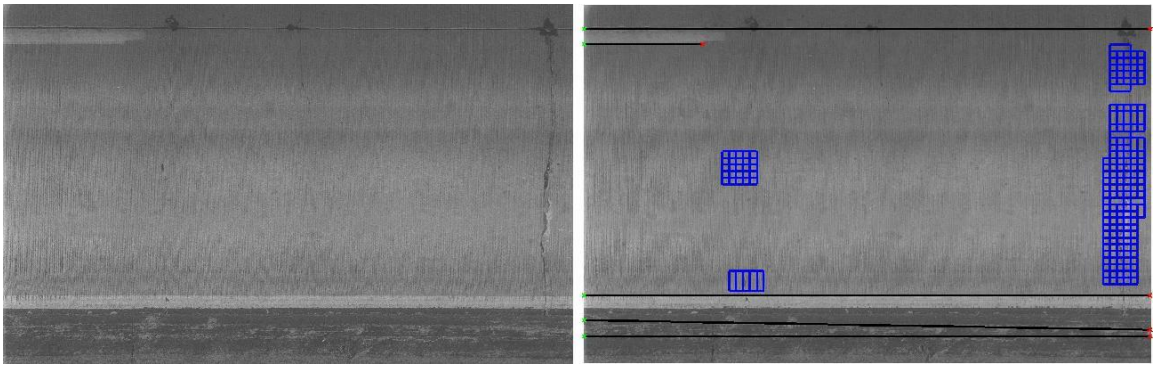

Figure 22. Example 3 of concrete crack at high severity: raw crack (left) and crack detection (right)

It is worth mentioning that Figure 22 (left) also contains a crack at low severity. The shape-based crack detection results from the three pavement images are presented in the right-hand images in Figure 20, Figure 21, and Figure 22.

We make the following observations from the detection results:

- Our approach has the capability to detect all cracks at high severity, although with some partial misses due to the small width of these crack segments.

- Our approach can also detects small black patches, as shown in Figure 20 (right), as well as thin crack segments at low severity, as shown in Figure 22 (right).

- Our approach also detects some raveling-type distress in the shoulder region beyond the joint. This can be explained by the fact that we employ constant parameters in our joint detection approach, which are not adaptive to various pavement datasets. In future work, more robust parameters are needed.

Detecting Medium-Severity Concrete Cracks

We give two examples of concrete cracks at medium severity in the left-hand images in Figure 23 and Figure 24.

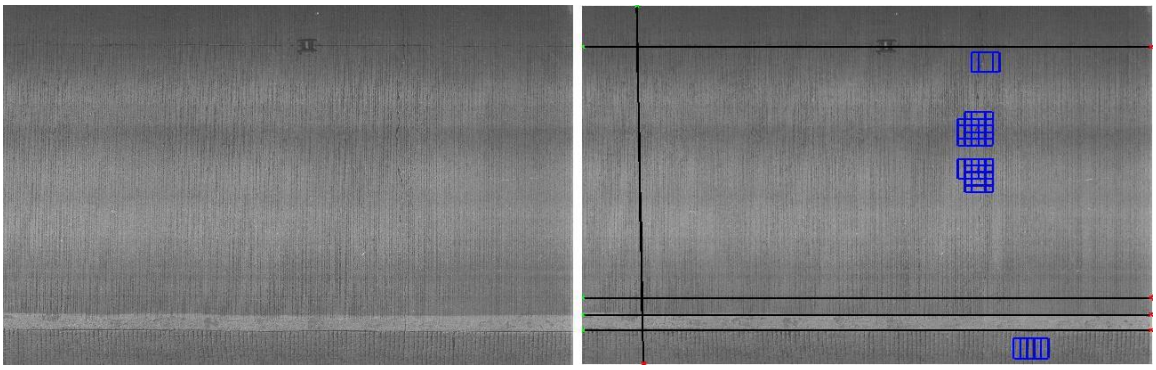

Figure 23. Example 1 of medium-severity concrete crack: raw crack (left) and crack detection (right)

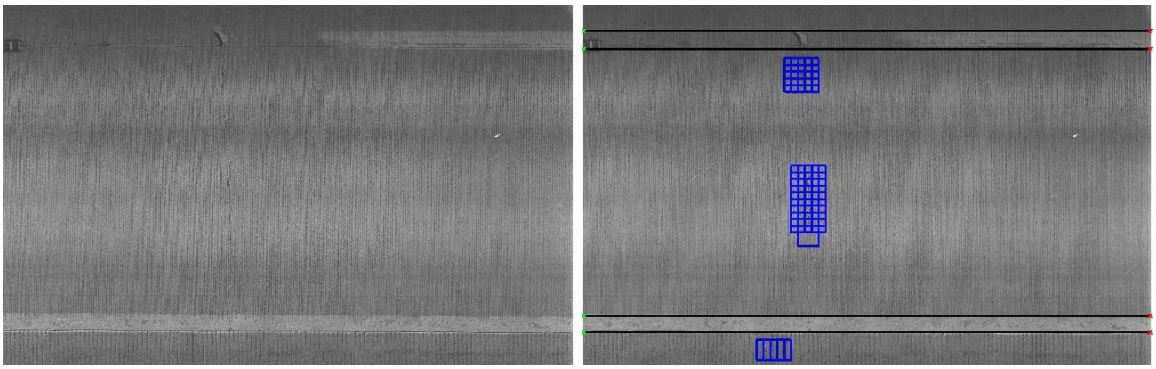

Figure 24. Example 2 of medium-severity concrete crack: raw crack (left) and crack detection (right)

The shape-based crack detection results from the two crack images are shown in the right-hand images in Figure 23 and Figure 24. Detection results show that our approach successfully detected both medium-severity cracks, with partial misses.

Detecting Low-Severity Concrete Cracks

We present two examples of low-severity concrete cracks in the left-hand images in Figure 25 and Figure 26

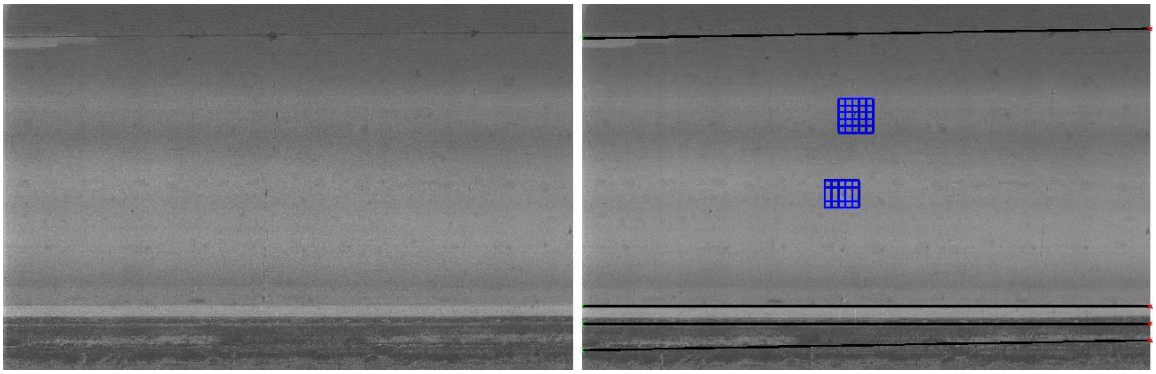

Figure 25. Example 1 of low-severity concrete crack: raw crack (left) and crack detection (right)

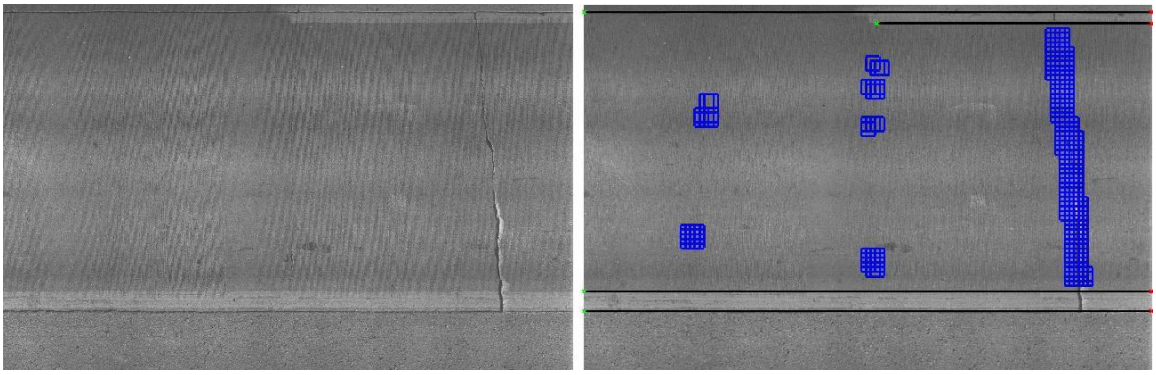

Figure 26. Example 2 of low-severity concrete crack: raw crack (left) and crack detection (right)

Figure 26 (left) contains one crack at high severity and two cracks at low severity, which can be seen by zooming into the image. The detection results of the two images are shown in the right-hand images in Figure 25 and Figure 26, respectively. We observe that the approach successfully detected all low-severity cracks as well as the high-severity concrete crack.

Dataset 3: Asphalt Pavement Images

In this section, we test our shape-based pavement detection approach on a set of asphalt pavement images at various severity degrees to test the performance of our approach.

Detecting High-Severity Asphalt Pavement Cracks

We give two examples of detecting high-severity asphalt pavement cracks in the left-hand images in Figure 27 and Figure 28.

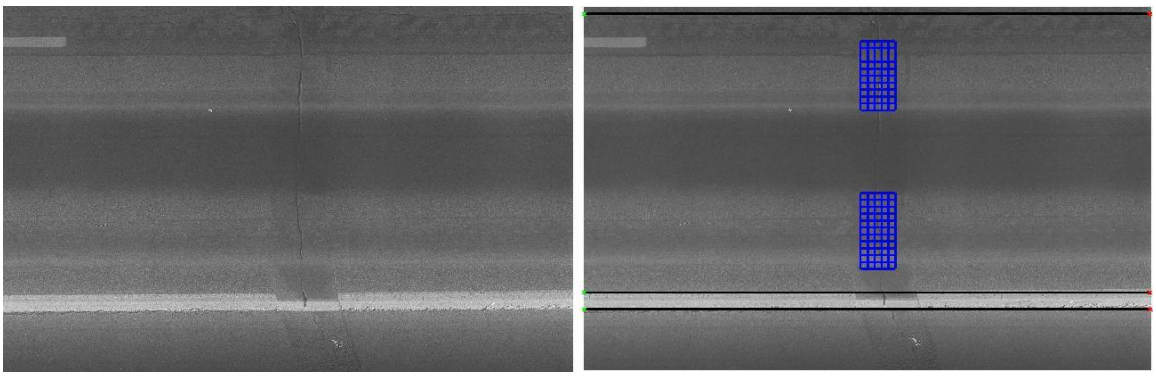

Figure 27. Example 1 of high-severity asphalt pavement crack: raw crack (left) and crack detection (right)

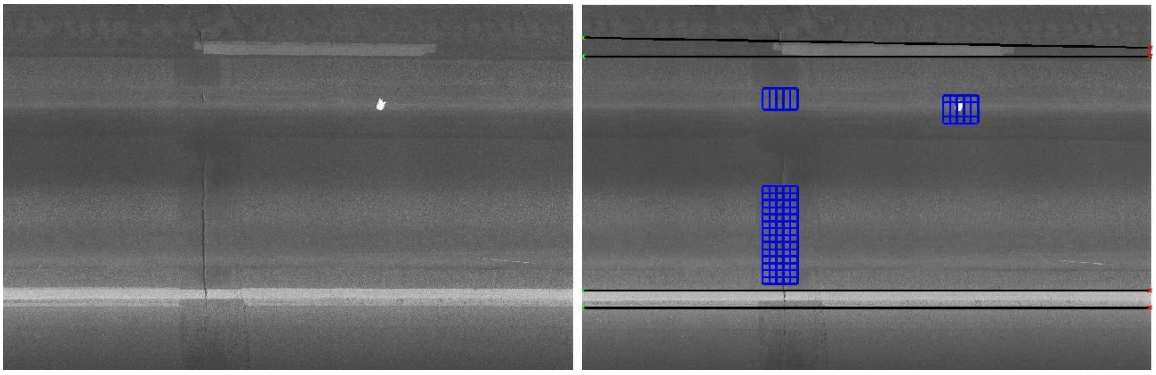

Figure 28. Example 2 of high-severity asphalt pavement crack: raw crack (left) and crack detection (right)

The detection results of the two crack images are presented in the right-hand images in Figure 27 and Figure 28, respectively. We make the observation that our approach successfully detected both high-severity cracks, although with some partial misses. Additionally, we get one false positive around the white patch. This can be explained as follows. The detection window enclosing the white patch has a high intensity contrast between the white patch and the background. After local filtering, the background is considered to be a crack pixel, and the bottom part at lower intensity values is extracted as the maximum connected component, whose shape resembles that of a crack.

Detecting Asphalt Pavement Cracks at Medium and Low Severities

We give an example of an asphalt pavement image containing two cracks, the top one at medium severity and the bottom one at low severity, in Figure 29 (left). The crack detection result from the image is shown in Figure 29 (right). We make the observation that the approach successfully detected both cracks, although with some partial misses.

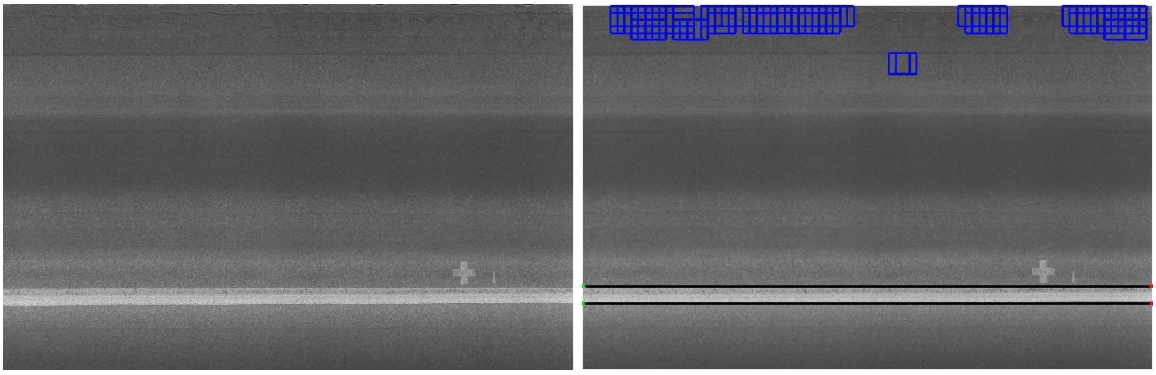

Figure 29. Example of longitudinal asphalt pavement cracks at medium and low severities: raw crack (left) and crack detection (right)

CRACK WIDTH COMPUTATION

Once the crack detection process is finished, we compute the width of each crack segment in order to classify the cracks. For each crack segment *CrackSeg* containing *W* detection windows, $CSWind^{(1)}$, $CSWind^{(2)}$,…,$CSWind^{(W)}$, we first compute the average crack width in each detection window $CSWind^{(i)}$. The details are as follows:

- Employ a top-hat filter to remove noise from the crack block.
- Employ the active contour method to segment the crack block into foreground and background regions and choose the one with the lower average intensity value as the crack region.
- Extract the connected component with the maximum area as the crack component.
- Compute the orientation of the crack segment and rotate the crack into a horizontal orientation.
- Compute the X-range (i.e., $x_{min}^{(i)}$, $x_{max}^{(i)}$) of the crack segment. For each $x \in \{x_{min}^{(i)}, \ldots, x_{max}^{(i)}\}$, compute the *y* difference of the crack, producing a set of *y* values $\{y_{x_{min}}^{(i)} \ldots y_{x_{max}}^{(i)}\}$.

The average crack width in the detection window $CSWind^{(i)}$ is defined as follows:

$$AveWCrckWidth^{(i)} = \frac{\sum_{x=x_{min}}^{x_{max}^{(i)}} y_x^{(i)}}{x_{max}^{(i)} - x_{min}^{(i)}} \tag{10}$$

Then the average width of the crack segment is computed as follows:

$$AveCrackWidth = \frac{\sum_{i=1}^{W} AveWCrckWidth^{(i)} \times (x_{max}^{(i)} - x_{min}^{(i)})}{\sum_{k=1}^{W} x_{max}^{(i)} - x_{min}^{(i)}} \tag{11}$$

An example of computing crack width in one detection window is presented in Figure 30.

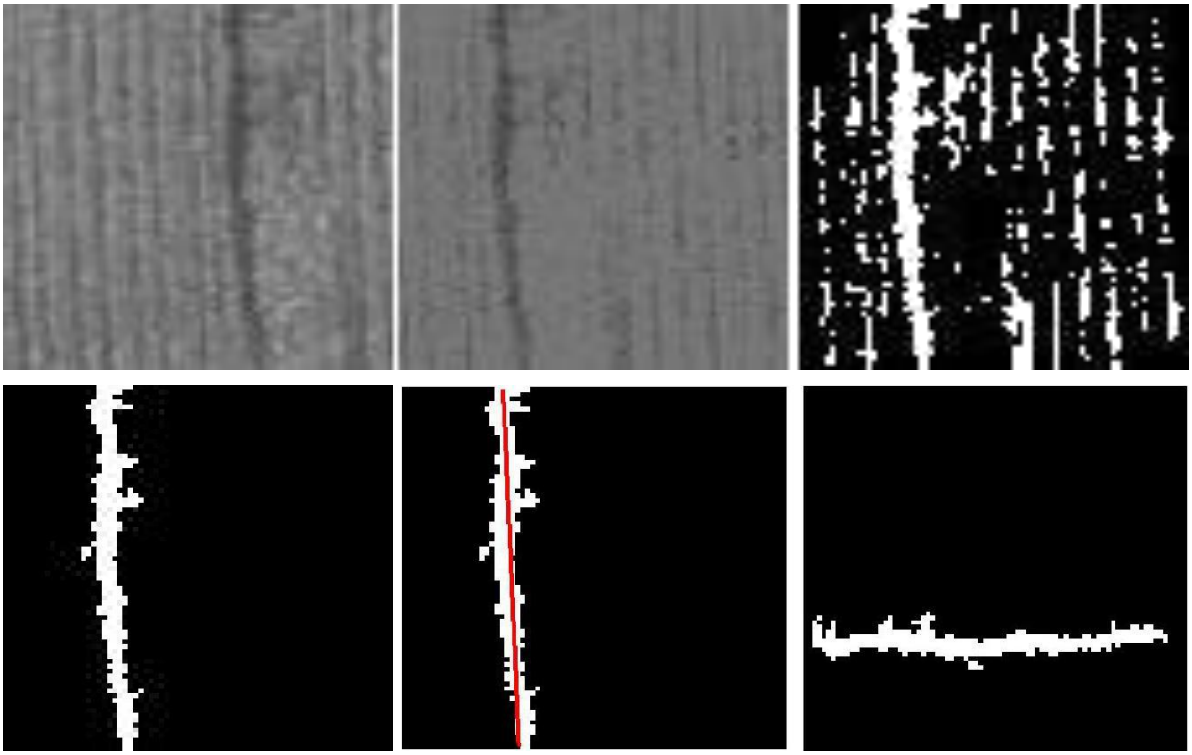

Figure 30. Steps in average crack width computation in a crack block (left to right, top row, then bottom row): crack block, top hat filter, segmentation, minor removal, computing orientation, and rotation

In Figure 30 (bottom center), fit crack pixels using a line and compute the orientation of the crack based on the line slope (92.5^{o} relative to horizontal axis). Based on Equation 10, the average crack width is computed as 4.53 pixels in this example. In addition, we show an example of computing the average width of the whole crack in Figure 31.

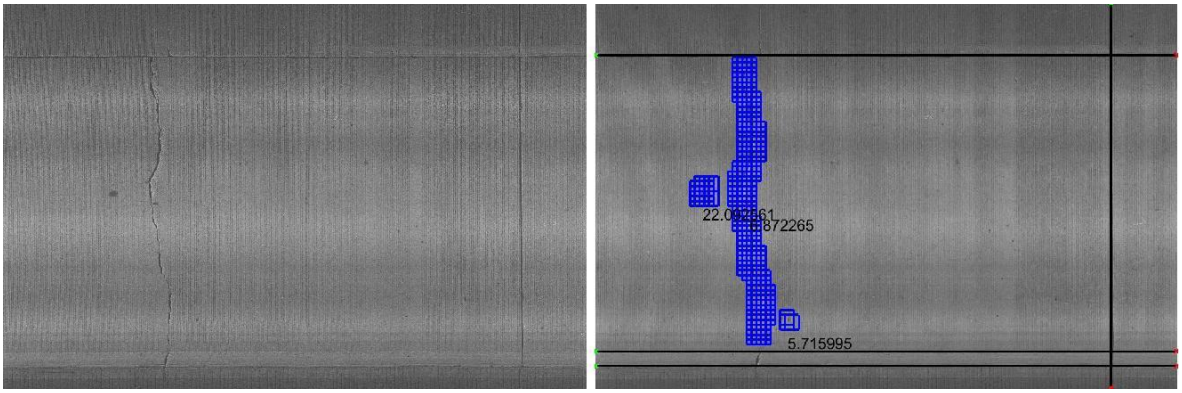

Figure 31. Example of crack width computation

The value in black below each segment represents the average width of the crack segment. The computed average widths of the left patch, middle crack, and right patch are 22.09, 6.87, and 5.71 pixels, respectively.

In addition, we test the crack width computation approach on cracks at different severity levels. The images on the left in Figure 32, Figure 33, and Figure 34 show examples of cracks at high, medium, and low severity, respectively.

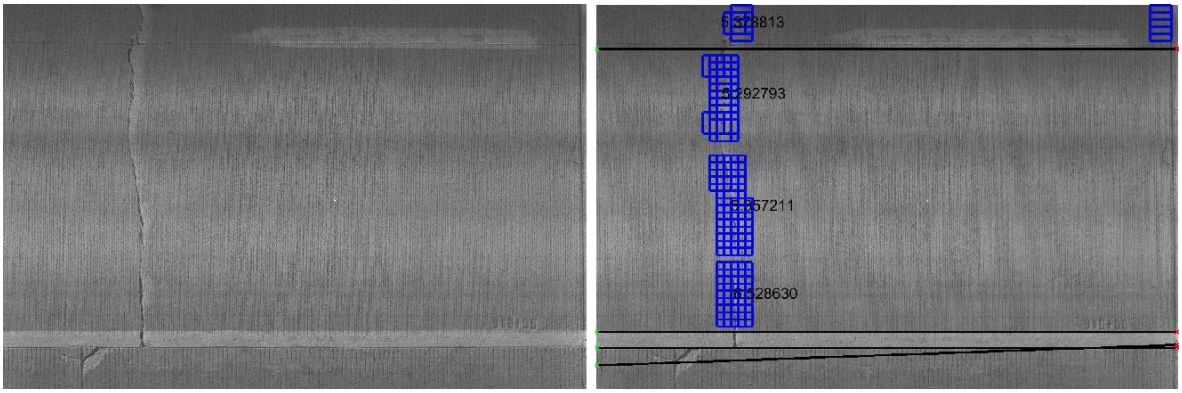

Figure 32. Example of computing crack width at high severity: raw crack (left) and crack detection (right)

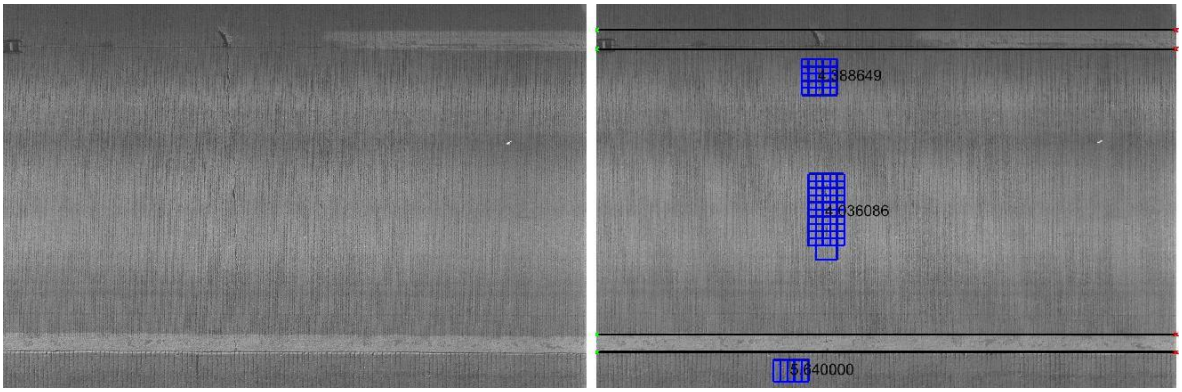

Figure 33. Example of computing crack width at medium severity: raw crack (left) and crack detection (right)

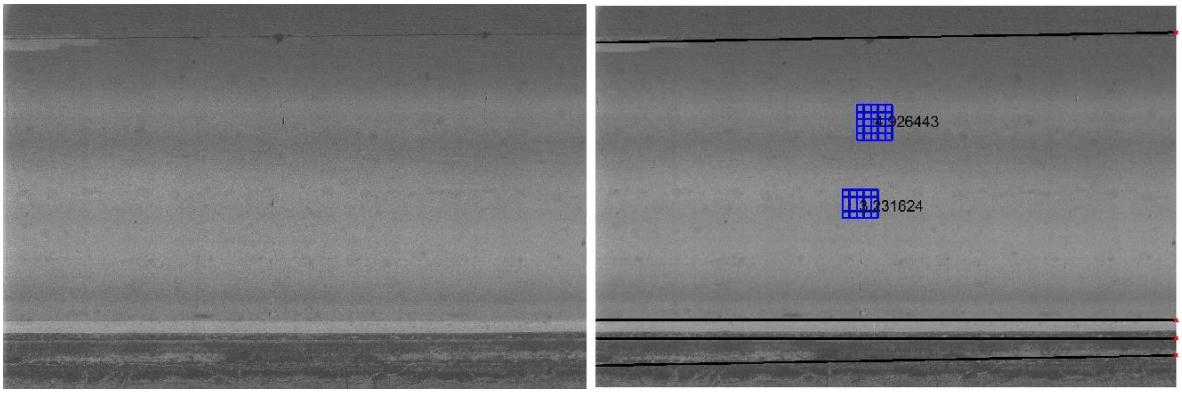

Figure 34. Example of computing crack at low severity: raw crack (left) and crack detection (right)

We employ the approach to compute the width of each crack segments and present the computation results in the right-hand images in Figure 32, Figure 33, and Figure 34. The results of the width computation satisfy our expectation that the widths of the crack segments at high severity are larger than those at medium and low severities.

SUMMARY

State highway agencies routinely employ highway-speed data-collection vehicles equipped with downward-looking digital cameras for the collection of network-level pavement images. These digital pavement images are then processed using proprietary semi-automated or fully automated image processing algorithms to identify pavement cracking information for reporting and use in pavement management systems for agency decision making regarding pavement preservation and rehabilitation.

Advancements are still being made in the development of accurate and reliable image-based pavement-crack-detection and classification algorithms. There is a need for the development of automated, low-cost crack detection algorithms that could be implemented by highway agencies for cost-effective and continuous roadway health monitoring and management.

The main objective of this proof-of-concept research was to develop a shape-based pavement-crack-detection approach for the reliable detection and classification of cracks from acquired 2D concrete and asphalt pavement images. Concrete and asphalt pavement JPEG images acquired through the 2D-area-scanning digital-imaging method (dimensions of 3,072 x 2,048 pixels) were used for the analysis.

The developed pavement-crack-detection approach takes advantage of the spatial distribution of crack pixels and works on each pavement image block of 75 by 75 pixels. The overall crack detection algorithm consists of four stages: local filtering, maximum component extraction, polynomial fitting of possible crack pixels, and shape metric computation and filtering. After completing the crack detection process, the width of each crack segment is computed to classify the cracks.

In order to verify the developed crack detection approach, a series of experiments was conducted on real pavement images without and with cracks at different severities. The developed shape-based pavement-crack-detection algorithm was able to detect cracks at different severities from both asphalt and concrete pavement images. Further, the developed algorithm was able to compute crack widths from the images for crack classification and reporting purposes.

Additional research is needed to improve the robustness and accuracy of the developed approach in the presence of anomalies and other surface irregularities.

REFERENCES

Adarkwa, O. A., and Attoh-Okine, N. 2013. Pavement Crack Classification Based on Tensor Factorization. *Construction and Building Materials*, 48, pp. 853-857.

Ahuja, N., and Barkan, C. 2007. *Machine Vision for Railroad Equipment Undercarriage Inspection Using Multi-Spectral Imaging*. Final Report for High-Speed Rail IDEA Project 49. Transportation Research Board, Washington, DC. Available at: http://onlinepubs.trb.org/onlinepubs/archive/studies/idea/finalreports/highspeedrail/hsr-49final_report.pdf.

Chen, L., Zhang, J., and Ji, R. 2009. Identification Algorithm for Pavement Cracks Based on Support Vector Machine. International Conference on Transportation Engineering (ICTE 2009), American Society of Civil Engineers (ASCE), Reston, VA.

Elkrry, A. M., and Anderson, N. 2013. *Non-invasive Imaging and Assessment of Pavements*. RiP Project 34542. Missouri University of Science & Technology, Rolla, MO. Available at http://transportation.mst.edu/media/research/transportation/documents/R329%20Final%20Report.pdf.

Flintsch, G., and McGhee, K. 2009. *Quality Management of Pavement Condition Data Collection*. NCHRP Synthesis 401. Transportation Research Board, Washington, DC. Available at http://onlinepubs.trb.org/onlinepubs/nchrp/nchrp_syn_401.pdf Accessed December 5, 2014.

Liang, S., and Sun, B. Using Wavelet Technology for Pavement Crack Detection. *ICLEM 2010: Logistics for Sustained Economic Development*. American Society of Civil Engineers (ASCE), Reston, VA.

McNeil, S., and Humplick, F. 1991. Evaluation of Errors in Automated Pavement-Distress Data Acquisition. *Journal of Transportation Engineering*, 117 (2): 224–241.

McGhee, K. H. 2004. *Automated Pavement Distress Collection Techniques*. NCHRP Synthesis 334. Transportation Research Board, Washington, DC.

McQueen, J. M., and Timm, D. H. 2005. Statistical analysis of automated versus manual pavement condition surveys. *Transportation Research Record: Journal of the Transportation Research Board*, 2004: 55–62.

Miller, J. S., and Bellinger, W. Y. 2003. *Distress Identification Manual for the Long-Term Pavement Performance Program*. FHWA-RD-03-031, Fourth Revised Edition. Federal Highway Administration, Washington, DC.

Neubauer, S., and Todsen, M. 2014. *Acoustic Imaging System Evaluation*. RiP Project 35756. Iowa Department of Transportation, Ames, Iowa. Project abstract available at http://rip.trb.org/view/2013/P/1278156.

Oliveria, H., and Correia, P. L. 2009. Automatic Road Crack Segmentation Using Entropy and Image Dynamic Thresholding. *Proceedings of the 17th European Signal Processing Conference (EUSIPCO 2009)*. Glasgow, Scotland. Available at http://www.eurasip.org/Proceedings/Eusipco/Eusipco2009/contents/papers/1569192726.pdf.

Peng, B., Wang, K. C. P., and Chen, C. 2014. Automatic Crack Detection by Multi-Seeding Fusion on 1 mm Resolution 3D Pavement Images. *Proceedings of the ASCE T&DI Congress*. American Society of Civil Engineers (ASCE), Reston, VA.

Pierce, L. M., and McGovern, G. 2014. *Implementation of the AASHTO Mechanistic-Empirical Pavement Design Guide and Software*. NCHRP Synthesis 457. Transportation Research Board, Washington, DC.

Roque, R. 2014. *Application of Imaging Techniques to Evaluate Polishing Characteristics of Aggregates*. RiP Project 36638. University of Florida, Gainsville. Project abstract available at http://rip.trb.org/view/2014/P/1312272.

Sun, B.-C., and Qiu, Y.-J.. 2007. Automatic Identification of Pavement Cracks Using Mathematical Morphology. International Conference on Transportation Engineering (ICTE 2007), American Society of Civil Engineers (ASCE), Reston, VA.

Vavrik, W., Evans, L., Sargand, S., and Stefanski, J. 2013. *PCR Evaluation – Considering Transition from Manual to Semi-Automated Pavement Distress Collection and Analysis*. Ohio Department of Transportation, Columbus, OH. Available at http://www.dot.state.oh.us/Divisions/Planning/SPR/Research/reportsandplans/Reports/2013/Pavements/134668_FR.pdf. Accessed December 5, 2014.

Wang, K. C. P. 2014. *Safety Evaluation of Pavement Surface Characteristics with 1mm 3D Laser Imaging*. Oklahoma State University, Stillwater, OK.

Wang, K. C. P., and Li, J. Q. 2014. *3D Laser Imaging for ODOT Interstate Network at True 1-mm Resolution*. Oklahoma Department of Transportation Materials and Research Division, Oklahoma City, OK. Available at http://ntl.bts.gov/lib/55000/55300/55359/FHWA-OK-14-14_2251_Wang.pdf .

Wei, H., Abrishami, H., Xiao, X., and Karteek, A. 2014. *Adaptive Video-based Vehicle Classification Technique for Monitoring Traffic*. University of Cincinnati, Cincinnati, OH. Available at http://ntl.bts.gov/lib/55000/55600/55640/Adaptive_Videobased_Vehicle_Classification_Technique_for_Monitoring_Traffic.pdf.

Zhang, J., Sha, A., Sun, Z. Y., and Gao, H. G. 2009. Pavement Crack Automatic Recognition Based on Weiner Filtering. *ICCTP2009: Critical Issues in Transportation Systems Planning, Development, and Management*. American Society of Civil Engineers (ASCE), Reston, VA.

Zimmerman, K., Smadi, O., Senesi, C., Kebede, N., and Shah, K. 2013. *Increasing Consistency in the Highway Performance Monitoring System for Pavement Reporting*. Final Report. NCHRP Project 20-24(82). Available at http://onlinepubs.trb.org/onlinepubs/nchrp/docs/NCHRP20-24%2882%29_FR.pdf. Accessed December 5, 2014.

Zou, Q., Cao, Y., Li, Q., Mao, Q., and Wang, S. 2012. CrackTree: Automatic Crack Detection from Pavement Images. *Pattern Recognition Letters*, 33 (3), pp. 227-238.